11 Instrumentation and Technique

11-1 A Novel Lattice-spacing Comparator with Resolution of 10^{-9}

In all fundamental theories there appear a number of parameters which characterize the fundamental particles and their interactions in nature: the fundamental physical constants. Avogadro's number N_A is one of them, and represents a bridge from the microscopic world to the macroscopic one. Knowledge of N_A to high precision would allow us to redefine the kilogram, which at present is defined by material artifact, the only definition of a base unit of the SI that has remained unchanged since 1889.

A very accurate way to determinate N_A is the X-ray crystal density method. A silicon crystal made with the floating-zone method (FZ-Si) is selected. The basic relationship between N_A and the experimental values is given by

$$N_A = 8M(\mathrm{Si}) / \{\rho(\mathrm{Si})\, a^3\} \quad (1)$$

where M(Si) is the molar mass of Si, a^3 is the unit cell volume of the crystal, ρ(Si) is density of the crystal and 8 represents the number of atoms in a unit cell of Si crystal. Here the absolute value of the silicon lattice parameter and information of its relative variation in the real crystal are necessary. The former can be measured by X-ray and optical interferometers with an uncertainty of 2×10^{-8}. However, the value of the d-spacing is an average obtained from the limited volume of the crystal, which is only one in hundreds of thousands that of a kilogram silicon sphere. Thus it is required to have a path to link the absolute d-spacing at locations throughout the crystal. For this purpose, a novel, fast and stable crystal lattice-spacing comparator has been developed at the Photon Factory which can complete one measurement process within thirty seconds for both d-spacing and lattice plane orientation [1]. The comparator, constructed at BL-3C2, is shown in Fig. 1. A fine collimated monochromatic beam with wavelength of 1.1778Å is selected by a monolithic double-crystal monochromator (MDCM) and pairs of 911 and $9\bar{1}\bar{1}$ diffractions employed. The interplanar angle β of (911) and ($9\bar{1}\bar{1}$) in the MDCM is 17.86028°, which can be accurately calculated from the cubic silicon crystalline symmetry, so the wavelength can be calculated accurately from the d-spacing at a certain temperature. When an X-ray beam with wavelength of 1.11778 Å is incident along [100] of the sample, the Bragg condition for the 911 and $9\bar{1}\bar{1}$ reflections is quasi-simultaneously satisfied. The relative d-spacing of the sample is given by

$$\Delta d/d = (P_1 - P_2) / 2\tan\theta_B = \gamma / 2\tan\theta_B, \quad (2)$$

where θ_B is Bragg angle of 81.02°, P_1 and P_2 are the peak positions of the twin peaks, and γ is the differential angle of the twin peaks. The variation in lattice plane orientation of the sample is given by

$$\Delta\alpha = (P_1 + P_2) / 2 - \alpha_0, \quad (3)$$

where α_0 is the initial angular position reading from the autocollimator.

The results of 200 measurements of the relative d-spacing at one spot of the sample are shown in Fig. 2. The standard deviation σ is 1.4×10^{-9}, showing that the resolution of the comparator has been improved

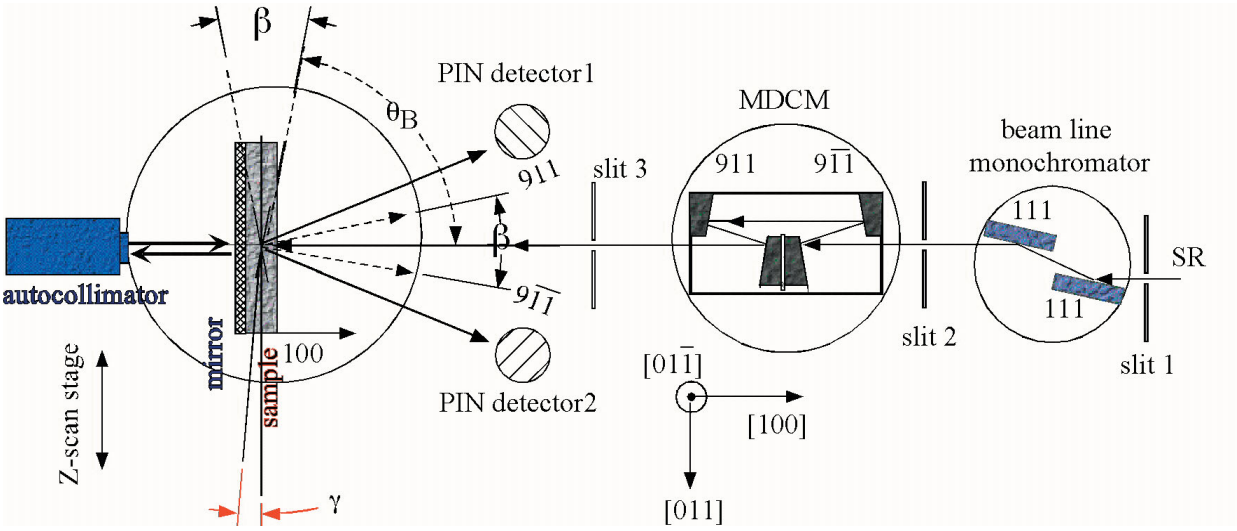

Figure 1
Schematic side view of the experimental arrangement. From the right, the Si (111) beamline monochromator, a monolithic double-crystal monochromator (MDCM) with wavelength of 1.1778Å which selects a fine collimated monochromatic beam, a piece of silicon sample with normal direction of [100], and goniometer for the sample. Two PIN photodiode detectors were used for measuring the intensity of 911 and $9\bar{1}\bar{1}$ diffractions. Angle β is the interplanar angle of (911) and ($9\bar{1}\bar{1}$), and angle γ is the interval of the two Bragg peaks $P_1$and P_2. A mirror mounted on the sample holder and an autocollimator are equipped for determining the projection of the local lattice plane orientation on the scattering plane.

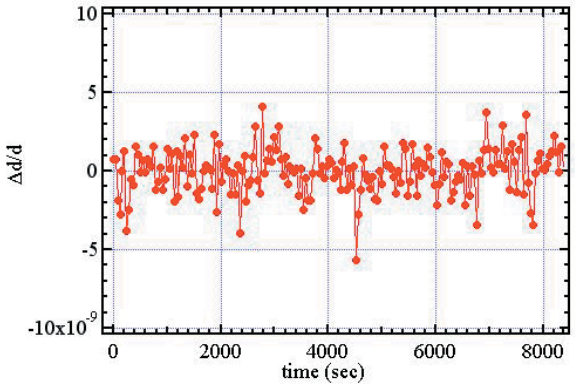

Figure 2
Experimental results of relative d-spacing obtained from 200 rocking-curve measurements within 130 minutes. The standard deviation of these 200 values is 1.4×10^{-9} and corresponds to the resolution power and stability of the comparator system.

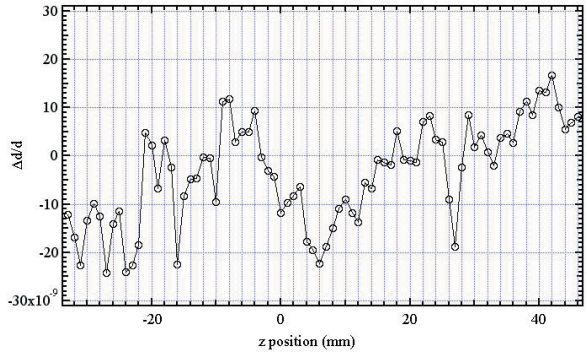

Figure 3
d-spacing measurement along a diameter of a 4-inch FZ-Si plate.

by a factor of ten compared to our previous work [1]. $\Delta d/d$ as a function of the position along a diameter of an FZ-Si sample is shown in Fig. 3. It is clear that the d-spacing of FZ-Si is not homogeneous on a scale of 10^{-8}, so the mapping of this measurement can provide an image of swirl defects even in low oxygen and carbon concentration FZ-Si.

X. W. Zhang (KEK-PF)

Reference

[1] X. W. Zhang, H. Sugiyama, M. Ando, Y. Imai and Y. Yoda, *J. Appl. Cryst.*, **36** (2003) 188.

11-2 An Angle-resolved Photoemission Study of 1*T*-TaS_xSe_{2-x} Using a Multi-axis Cryogenic Sample Manipulator

Optical excitation processes in condensed matter are governed by the symmetry of both the band states and the electronic dipole operator, because the transition probability ($P_{f\leftarrow i}$) from an initial state (φ_i) to a final state (φ_f) is given by the Fermi's golden rule:

$$P_{f\leftarrow i} \propto \left|\int \varphi_f \vec{e}\cdot\vec{r}\,\varphi_i d\tau\right|^2,$$

where $\vec{e}\cdot\vec{r}$ is the dipole operator. Therefore angle-resolved photoemission spectroscopy (ARPES) using polarized radiation can determine the symmetry of the initial states of condensed matter based on the symmetry selection rules. It offers the key to an understanding of the essential electronic structure. Although synchrotron radiation is ideal for polarization-dependent ARPES measurements, not many investigations have been performed so far, because it is technically difficult to control the direction of a sample sufficiently. Recently, we have developed a three-axis cryogenic sample manipulator suitable for ARPES as shown in Fig. 4 [1], and installed it in the ARPES apparatus with an electron spectrometer mounted on a two-axis goniometer. The polar, azimuth and tilt rotations of the sample can be controlled independently. Continuous 360˚ rotation around the polar axis, azimuthal rotation of up to ±180˚ and tilt rotation from +95˚ to -5˚, measured from the plane normal to the polar axis, are possible. Nonmagnetic materials are used near the sample holder of the manipulator. With liquid nitrogen and liquid helium for the cryostat, the sample is cooled down to 90 and 12.5 K, respectively.

We have studied the detailed electronic structure of layered transition-metal dichalcogenides 1*T*-TaS_xSe_{2-x}, and demonstrated the validity of polarization-dependent ARPES with a multi-axis cryogenic sample manipulator [2-4]. The ARPES measurements were carried out at BL-1C. Fig. 5 shows azimuth dispersion spectra of 1*T*-$TaS_{1.2}Se_{0.8}$ for different parallel momenta using p-polarized light and s-polarized light [3]. A drastic reduction in the spectral weight along the high symmetry line ΓM, particularly around the point M, was observed when s-polarized light was used. This implies that the initial state must be symmetric with respect to a mirror plane perpendicular to the line ΓK, consistent with conventional band calculations in the absence of the commensurate charge-density-wave (CDW). Based on a model calculation of the spectral function, which captures the main features of the ARPES spectra quite well qualitatively [4], we conclude that there is only a limited amount of modification in the electronic structure of 1*T*-TaS_xSe_{2-x} caused by the CDW-related potential and that the metal-insulator transition in 1*T*-TaS_xSe_{2-x} is driven by the narrowing of the band width of the Ta 5d band straddling the Fermi level, which is induced by the increase in the CDW-related potential.

We have shown that the polarization-dependent ARPES method combined with the multi-axis cryogenic sample manipulator gives crucial information for understanding the electronic structure of quasi-two-dimensional materials.

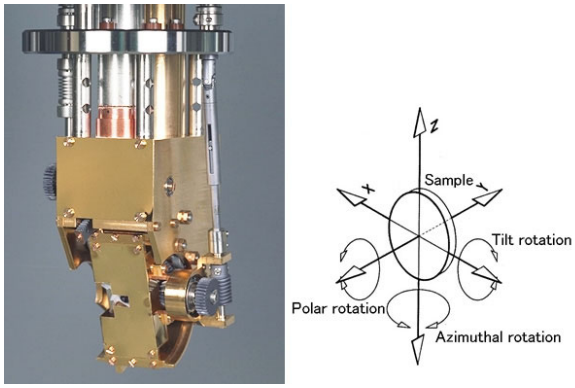

Figure 4
A photograph of the manipulator near the sample.

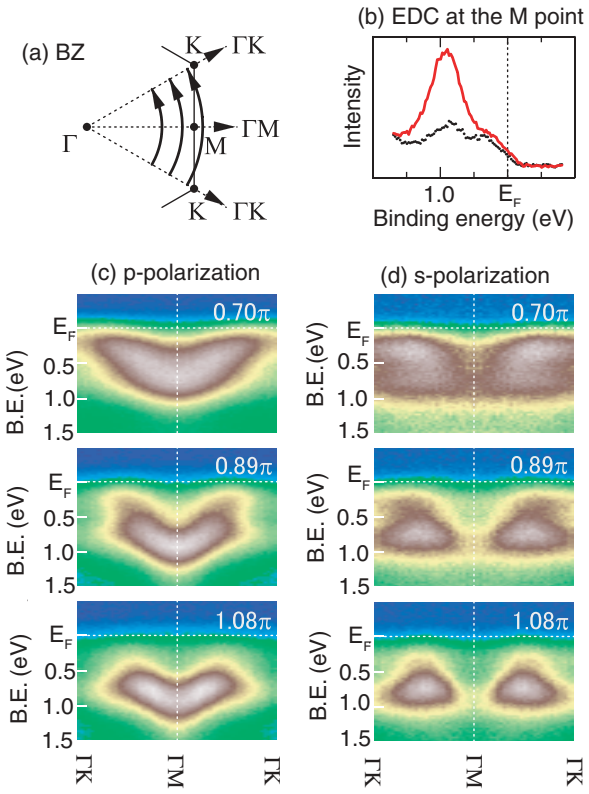

Figure 5
(a) Sketch of the arcs where spectra have been taken with fixed momenta of 0.70π, 0.89π, and 1.08π. BZ represents the Brillouin zone. (b) Energy distribution curve (EDC) spectra at the M point using p-polarized light (solid red curve) and s-polarized light (dotted curve). Azimuth dispersion spectra for fixed momenta of 0.70π, 0.89π, and 1.08π using (c) p-polarized light and (d) s-polarized light. Spectra start in the ΓK direction and end in the next ΓK direction via the ΓM direction. All spectra were recorded with $h\nu$ = 40 eV and T = 300 K. B. E. represents binding energy.

Y. Aiura[1], H. Bando[1], K. Yagi-Watanabe[1], K. Ozawa[2] and K. Ono[3] ([1]AIST, [2]Tokyo Inst. of Tech., [3]KEK-PF)

References

[1] Y. Aiura, H. Bando, T. Miyamoto, A. Chiba, R. Kitagawa, S. Maruyama and Y. Nishihara, *Rev. Sci. Instrum.* **74** (2003) 3177 .
[2] Y. Aiura, H. Bando, R. Kitagawa, S. Maruyama, Y. Nishihara, K. Horiba, M. Oshima, O. Shiino and M. Nakatake, *Phys. Rev. B* **68** (2003) 073408.
[3] Y. Aiura, I. Hase, H. Bando, K. Yagi-Watanabe, K. Ozawa, T. Iwase, Y. Nishihara, O. Shiino, M. Oshima, M. Kubota and K. Ono, *Phys. Rev. Lett.* **91** (2003) 256404.
[4] Y. Aiura, I. Hase, K. Yage-Watanabe, H. Bando, K. Ozawa, K. Tanaka, R. Kitagawa, S. Maruyama, T. Iwase, Y. Nishihara, K. Horiba, O. Shiino, M. Oshima, M. Nakatake, M. Kubota and K. Ono, *Phys. Rev. B* **69** (2004) 245123.

11-3 X-ray Nonreciprocal Directional Dichroism of a Polar Ferrimagnet

Left- and right-handed circularly polarized light encounter different absorption coefficients in a ferromagnetic solid (Faraday effect). When the inversion symmetry is further broken, a novel magneto-optical effect, termed nonreciprocal directional dichroism or magneto-chiral dichroism, is expected to appear [1-2]. In the case of a polar ferromagnet (or polar ferrimagnet), the X-ray nonreciprocal directional dichroism (XNDD) effect is described as the phenomenon that X-ray absorption depends on whether the k vector is parallel or anti-parallel to the outer-product $P \times M$ under the preservation of mirror symmetry. P and M denote the electric polarization and spontaneous magnetization vectors, respectively. The most probable origin of the XNDD spectra is the interference between electric dipole and quadrupole processes through a spin-orbit coupling and a breaking of the parity through noncentrosymmetric crystal structure.

We have successfully detected the first signal of XNDD effect in a polar ferrimagnet $GaFeO_3$ at BL-1A [3]. The crystal structure of $GaFeO_3$ is illustrated in Fig. 6(a). An electric polarization is generated along the b axis, while a magnetic easy-axis is parallel to the c axis. Fig. 6(b) shows the experimental configuration for the observation of XNDD. XNDD is observed as the first-harmonic component of the transmission intensity $I_1(f)$, responding to the magnetic field with a lock-in amplifier. Fig. 7(a) shows X-ray absorption spectra of $GaFeO_3$ recorded at 50 K in the vicinity of the Fe K-edge for X-ray polarizations (E^{ω}) parallel to b and c. The bump at about 7.113 keV corresponds to transitions from Fe 1s to Fe 3d (pre-edge), and the local maximum at about 7.130 keV corresponds to transitions from Fe 1s to Fe 4p (main edge). Spectra showing XNDD at 50 K are shown in Fig. 7(b). The magnitudes of the XNDD effect around the pre-edge are comparable for $E^{\omega} // b$ and $E^{\omega} // c$, while the sign is opposite. XNDD is much larger around the pre-edge than around the main edge for the both X-ray polarizations. This indicates that the quadrupole transition from Fe 1s to Fe 3d plays an important role in this novel phenomenon.

The XNDD process is sensitive not only to the magnetic moment but also to the local symmetry, and hence can probe the local magnetization at the site of broken symmetry. Therefore, XNDD spectroscopy may find a broad range of applications to the characterization of

interface magnetism, such as the magnetic junctions/interfaces of the magneto-resistive sensors and memories, which would be otherwise difficult to probe.

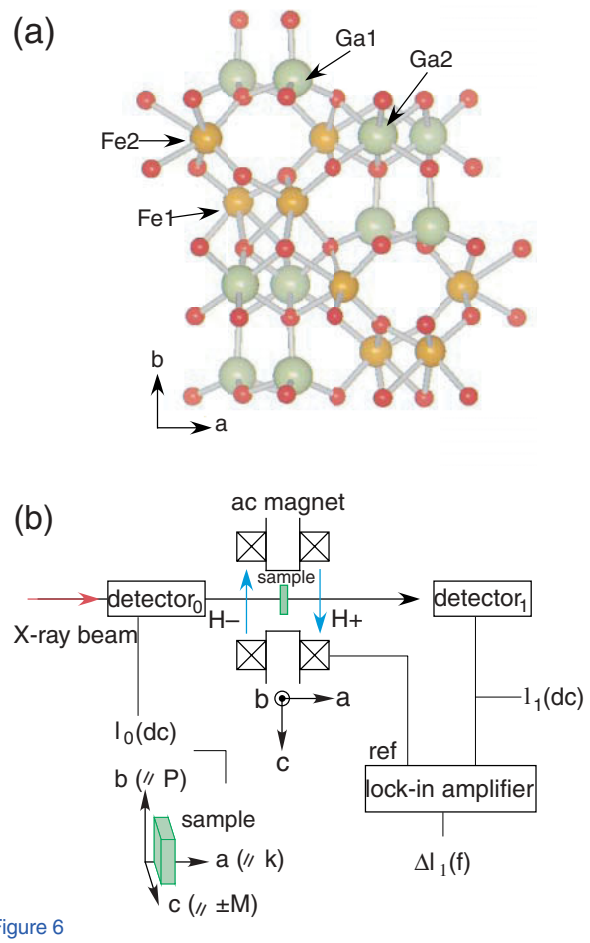

Figure 6
(a) Crystal structure of $GaFeO_3$. An electric polarization appears along the *b* axis, which causes the breaking of inversion symmetry, while the *c* axis is a magnetic easy-axis. (b) Experimental configuration for the observation of XNDD. Linearly-polarized X-ray is injected onto the (100) plane, while an alternating magnetic field is applied along the *c* axis in the Voigt configuration.

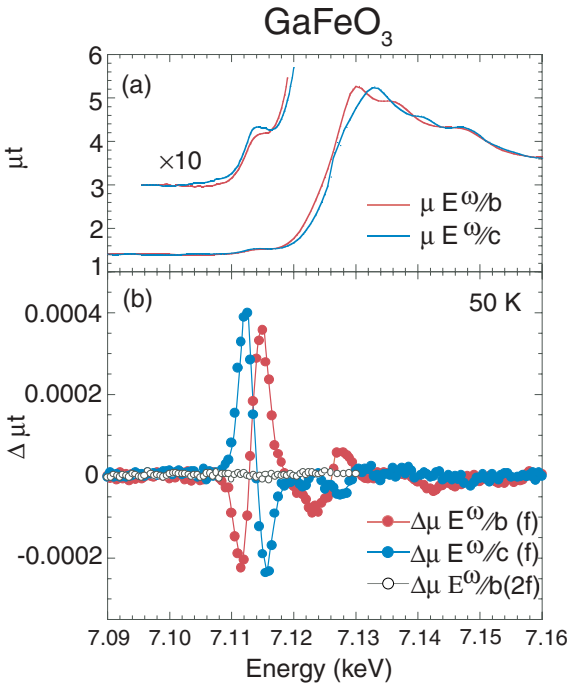

Figure 7
Spectra of (a) the X-ray absorption μt and (b) the XNDD $\Delta\mu t$ of a $GaFeO_3$ crystal at 50 K for E^{ω} // *b* (red) and E^{ω} // *c* (blue). $\Delta\mu t$ is defined as the difference of absorption coefficients when a magnetic field is applied parallel and anti-parallel to the *c* axis.

M. Kubota[1], T. Arima[2,3], Y. Kaneko[2], J. P. He[2], X. Z. Yu[2] and Y. Tokura[2,4,5]([1]KEK-PF, [2]ERATO-JST, [3]Tohoku Univ., [4]Univ. of Tokyo, [5]CERC-AIST)

References

[1] W.F. Brown, Jr. S. Shtrikman and D. Treves, *J. Appl. Phys.*, **34** (1963) 1233.
[2] R.V. Pisarev, *Sov. Phys. JETP* **31** (1970) 761.
[3] M. Kubota, T. Arima, Y. Kaneko, J.P. He, X.Z. Yu and Y. Tokura, *Phys. Rev. Lett.*, **92** (2004) 137401.